Sputtered Tungsten-Based Ternary and Quaternary Layers for Nanocrystalline Diamond Deposition

Michael J. Walock[1, 2, *], Issam Rahil[2], Yujiao Zou[1], Luc Imhoff[3], Shane A. Catledge[1], Corinne Nouveau[2], and Andrei V. Stanishevsky[1]

[1] *Dept. of Physics, University of Alabama at Birmingham, Birmingham, AL 35294, USA*
[2] *Laboratoire Bourguignon des Matériaux et Procédés, CER Arts et Métiers ParisTech of Cluny, 71250 Cluny, France*
[3] *Laboratoire Interdisciplinaire Carnot de Bourgogne, UMR 5209 CNRS-Université de Bourgogne, 21078 Dijon, France*

Many of today's demanding applications require thin-film coatings with high hardness, toughness, and thermal stability. In many cases, coating thickness in the range 2–20 μm and low surface roughness are required. Diamond films meet many of the stated requirements, but their crystalline nature leads to a high surface roughness. Nanocrystalline diamond offers a smoother surface, but significant surface modification of the substrate is necessary for successful nanocrystalline diamond deposition and adhesion. A hybrid hard and tough material may be required for either the desired applications, or as a basis for nanocrystalline diamond film growth. One possibility is a composite system based on carbides or nitrides. Many binary carbides and nitrides offer one or more mentioned properties. By combining these binary compounds in a ternary or quaternary nanocrystalline system, we can tailor the material for a desired combination of properties. Here, we describe the results on the structural and mechanical properties of the coating systems composed of tungsten-chromium-carbide and/or nitride. These WC-Cr-(N) coatings are deposited using magnetron sputtering. The growth of adherent nanocrystalline diamond films by microwave plasma chemical vapor deposition has been demonstrated on these coatings. The WC-Cr-(N) and WC-Cr-(N)-NCD coatings are characterized with atomic force microscopy and SEM, X-ray diffraction, X-ray photoelectron spectroscopy, Raman spectroscopy, and nanoindentation.

Keywords:

1. INTRODUCTION

In the context of industrial coatings on tools, machine parts, and biomedical implants, there are many key factors involved in their development. The coatings must be hard and tough; they must be chemically resistant and thermally stable. In some applications, they must also be biocompatible. In almost all contexts, the films must meet an optimal thickness[1–5] often with very low surface roughness. One material meets almost all of these requirements: diamond. Single-crystal diamond (SCD) is extremely hard, chemically resistant, thermally stable, and biocompatible. However, the crystalline nature of diamond leads to a higher than desired surface roughness. Nanocrystalline diamond (NCD) consists of nano-sized crystallites of diamond with the grain boundaries containing non-diamond carbon. As a result, they share many of the same desirable characteristics as mono- or poly-crystalline diamond films, but with lower surface roughness and higher toughness.[6, 7]

However, as desirable as NCD films appear, there are drawbacks. It is difficult to grow adherent NCD films on many commercial substrates. To overcome this, significant surface modification is necessary. Here, there are two schools of thought: chemical or physical modification. For example, cemented WC substrates can be chemically etched with an H_2SO_4/H_2O_2, or HNO_3/H_2O, solution to remove the Co binder[8–11] before diamond film deposition.

Physical modification can take several paths, such as plasma pretreatment, nanoparticle seeding, or interlayer deposition. For example, plasma treatment can improve the activity of the substrate's surface layer.[12] In nanoparticle seeding, diamond (or SiC) nanoparticles act as growth centers for subsequent diamond deposition.[13–15] This can be further enhanced by applying a voltage bias to the seeded substrate during deposition.[16, 17] While it has been proven successful on many different substrates, seeding is

*Author to whom correspondence should be addressed.

time-consuming and can be expensive. Another option is the use of coatings to act as buffer layers between the substrate and the NCD coating. These underlayers are developed to act as a diffusion barrier, adhesion enhancement, and/or as a seed for NCD growth. For example, Si has been used as a diffusion barrier on stainless steel.[18] On cemented-WC substrates, both homogeneous carbides[19] and graded WC layers have been investigated.[20] Other approaches have included Al,[21] W-Al bilayers,[22] and Mo[23] thin films.

However, for maximum effectiveness, the underlayers must not degrade the characteristics of the NCD coating but should rather enhance them. In other words, they must also meet the stringent standards necessary for the NCD coating, i.e., high hardness and toughness, chemical and thermal stability, and possible biocompatibility. This can be achieved through the use of nanocomposite coatings. By moving to a nanocomposite, the material can be tailored for the desirable attributes.

A typical composite film consists of at least two materials with little or no solubility between the constituent phases. If the crystallite sizes are less than 10–20 nm, a nanocomposite is formed. The combination of multiple phases, with small crystallite size, leads to a change in the dislocation behavior.[24] In traditional materials, dislocations occur within the grains. In a nanocomposite, the grain size is limited and the dislocations occur at the grain boundaries. This limits the dislocation propagation and leads to significantly improved mechanical properties.

For example, single crystal diamond films are superhard, but have low toughness. In addition, their crystalline nature may lead to high surface roughness. To overcome these difficulties, a nanocomposite of graphitic C and diamond is formed: nanocrystalline diamond. However, adhesion is still an issue. Typically, significant surface modification is necessary for good adhesion to a wide variety of substrates.[8, 9, 15, 17, 18, 25, 26]

Nanocrystalline TiN combined with an amorphous SiN matrix has shown a hardness greater than diamond.[27–32] Other examples of nanocomposites may not reach superhardness, but are considered supertough, such as nc-TiC/a-C[33] and nc-WC/a-C.[34] While nc-diamond, nc-nitride/a-nitride, and nc-carbide/a-C nanocomposites have become well established, less information is available on nc-carbide/a-nitride nanocomposites.

In the present study, the viability of a Cr-WC-(N) based coating system is evaluated. This system was chosen as a result of the characteristics of the components. Binary WC is often prepared as tough and smooth crystalline film, but may have lower hardness than NCD films.[35, 36] WN is typically harder than WC, but more brittle.[37–40] CrN is excellent for wear and oxidation resistance,[41, 42] but can often form with a porous columnar structure.[43, 44] However, if properly combined, the resulting ternary and quaternary composites may act as a hard, tough, and smooth, thermally stable films. Additionally, it has been hypothesized that they may act as a seed layer for subsequent nanocrystalline diamond growth.

2. EXPERIMENTAL METHODS

2.1. Sample Preparation

The ternary and quaternary coatings were deposited by RF magnetron sputtering (Nordiko 3500), operating at 13.56 MHz, using 4-inch WC (Neyco, 99.5% pure) and Cr (Neyco, 99.95% pure) targets. The Si and Ti substrate temperatures were less than 200 °C during deposition. The system base pressure is 6×10^{-5} Pa, with a working pressure of 0.4 Pa. The working gas was either pure Ar or an Ar/N_2 mixture. Four sample compositions were produced: WC, CrWC, WCN, and CrWCN. The deposition conditions are summarized in Table I.

The NCD coatings were produced in a 6 kW, 2.4 GHz microwave chemical vapor deposition (MW-CVD, Wavemat) system. The system base pressure is 1.3 Pa. The working pressure was 5.3 kPa, with a gas mixture of 84% H_2, 1.5% N_2, and 14.5% CH_4. The deposition time was 7 hours. The NCD films are deposited directly onto the ternary and quaternary films, without seeding. The temperature was approximately 780 °C during deposition on Ti substrates and approximately 720 °C during deposition on Si substrates. Based on prior experience growing NCD with this apparatus,[45–47] the film thickness is approximately 2.5 μm.

2.2. Characterization

Once deposited, the samples were characterized with various techniques to determine the structural, chemical, and mechanical parameters of the films. A Philips X'pert thin film diffractometer system, operating with Cu K-α radiation ($\lambda = 0.15406$ nm) at 45 kV and 40 mA, was used to identify crystalline phases. While the detector was scanned between 20° and 80°, the source was kept at a 5° incident angle. Crystallite size was estimated using the Debye-Scherrer equation. The surface morphology was measured with an atomic force microscope (AFM, Veeco Topometrix Explorer) in contact mode at ambient temperature, pressure, and humidity. In addition, cross-sectional, high-resolution scanning electron microscopy (HR-SEM,

Table I. Summary of deposition conditions for ternary and quaternary films.

Film	P (Pa)	Time (min)	Ar/N_2 (%)	Voltage (V)		Buffer layer
				Cr	WC	
WC	0.4	187	100		−900	370 nm Cr
CrWC	0.4	187	100	−500	−500	170 nm Cr
WCN	0.4	187	60/40		−500	170 nm Cr
CrWCN	0.4	187	60/40	−500	−500	

JEOL JSM 6400F) was used to look at the growth mode and to determine the coating thickness. This field emission SEM used an accelerating voltage of 20 keV. The chamber pressure during measurement was less than 1×10^{-4} Pa.

A PHI 5000 Versaprobe imaging X-ray photoelectron spectrometer (XPS), operating a monochromatic, focused Al K-α X-ray source (E = 1486.6 eV) at 25 W with a 100 μm spot size, was used to determine the chemical bonding of the samples. The samples were grounded and charge neutralization was provided by a cold cathode electron flood source and low-energy Ar-ions. All measurements were taken at room temperature and at a pressure of 2×10^{-6} Pa; the system base pressure is 5×10^{-8} Pa. The energy scale was calibrated with reference to the Ag 3d peak. Surface contamination is removed with Ar-ion sputter etching for 1 min at 1 kV; this removes 2.6 nm from the surface. Surface cratering, due to sputter etching, is limited by rastering the beam across a 2×2 mm^2 area. Survey scans, with pass energy of 117.4 eV and 1 eV step size, and high-resolution scans, with pass energy of 23.5 eV and 0.2 eV step size, were taken both before and after surface cleaning by sputter-etching. The chemical compositions and bonding states of the films were determined using Multipak v9.0. Raman spectroscopy was used to determine the carbon bonding states in both the as-prepared underlayers and the NCD coated films. This system (Dilor XY) uses a 300 mW solid state laser (Dragon Lasers), operating at $\lambda = 532$ nm, focused to a 10 μm spot size. All measurements were taken in standard laboratory conditions.

The mechanical properties of ternary and quaternary coatings were measured with a Nanoindenter XP (MTS Systems). Silica samples were used for calibration, and a Berkovich, total included angle of 142.3°, diamond indenter was used for all measurements. The maximum indentation depth was 500 nm. Hold times of 10 s (at maximum load) and 50 s (at 10% maximum during unloading) were used to minimize thermal drift and creep effects. The resulting measurements were processed with TestWorks 4 to produce load-displacement curves. The hardness and Young's modulus of each sample were calculated using the Oliver and Pharr method.[48] Due to soft substrates, both the hardness and the Young's modulus were estimated for the indentation depths in the range of 50–100 nm. This was approximately 5%–10% of the film thickness depending on the sample.[49]

3. RESULTS AND DISCUSSION

A binary WC sample was prepared on Si using the WC target, without the reactive gas. Figure 1(a) shows the XRD pattern for the WC sample on Si. By comparing this pattern with prior work[35] and the ICDD powder diffraction file (PDF) database,[50] the structure has been determined as carbon deficient, polycrystalline WC_{1-x} phase, with an average crystallite size of approximately 3 nm.

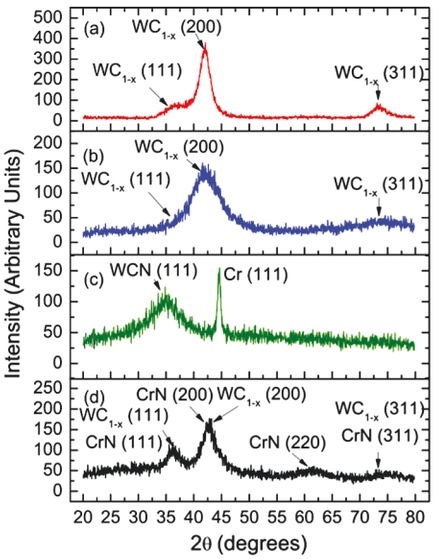

Fig. 1. X-ray diffraction pattern for the (a) WC, (b) CrWC, (c) WCN, and (d) CrWCN coatings, deposited on Si.

The Raman spectroscopy measurements (not shown) indicated the absence of free C in the film. After removing the surface contamination, the XPS results (not shown) only show two carbide states in C1s core level at 283.5 eV and 282.4 eV. Thus, the film may contain some amount of W_2C.

It has been found that the WC coatings prepared in this process partially delaminate from the most of the substrates used. However, the remaining adherent fragments of WC film were very smooth, with a RMS roughness of approximately 1.06 nm (as measured by AFM in 5×5 μm^2 area). The nanoindentation tests yielded a Young's modulus of 404 GPa, and a high hardness of 38 GPa.

The analysis of Cr-WC coatings is not quite as straight forward as the binary WC material. This is partly due to the lack of accepted data files within the ICDD database, and the limited literature on this combination of materials.[51,52] As shown in Figure 1(b), there is a single broad peak centered at $2\theta = 41.9°$. The breadth of this peak may be the result of significant overlap between WC_{1-x} and CrC phases. Unfortunately, this amount of overlap precludes an accurate estimate of the average grain size. XPS has been used to further resolve the structure and chemical bonding in the film. As shown in Figure 2(a), there is about 1.5 at. % of oxygen in the film located in two states at 530.0 eV and at 528.8 eV. In Figure 2(b), the C1s spectrum is split in two states at 283.2 eV and 281.7 eV. Both appear to be bound carbide states. Figure 2(c) shows that the $Cr2p^{1/2}$ and $Cr2p^{3/2}$ peaks are located at 581.9 eV and 572.5 eV, respectively. From the NIST XPS Database,[53] this is most likely a Cr_7C_3 phase. Finally, Figure 2(d) shows the W4d peaks, with two distinct states. The W4f peak (not shown) shows only one state. Thus, it has been suggested that the Cr-WC system consists of W-C and Cr-C phases, with a small amount of W-O.

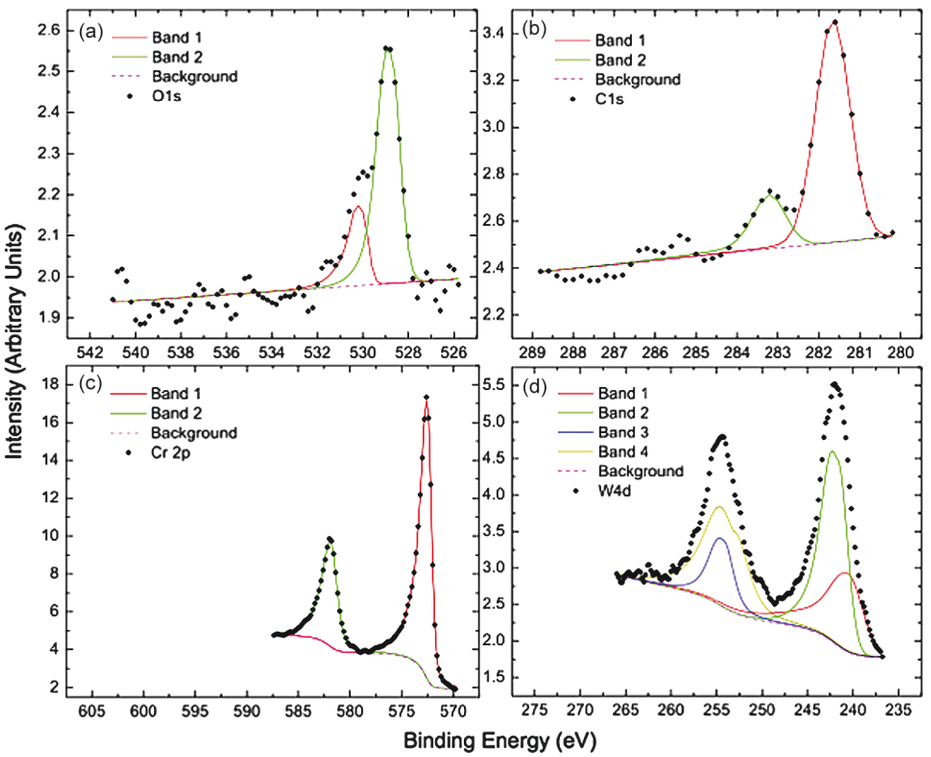

Fig. 2. X-ray photoelectron spectroscopy results for the (a) O1s, (b) C1s, (c) Cr2p, and (d) W4d peaks of the CrWC coating, deposited on Si. The symbols (♦) are the raw data, with the deconvoluted peaks (solid) and the iterated Shirley background (dashed).

While the Cr-WC coating is 1.5 μm thick, smooth, and adherent, its hardness and Young's modulus are 19 GPa and 263 GPa, respectively. One possible explanation for the reduced mechanical properties, compared to the binary WC, is oxygen contamination; there is approximately 1.5 at.% of oxygen in the film. While both WC and CrC are hard materials, oxides are typically not. For example, WO_x and WON have been reported with hardness values of only 7 GPa and 15 GPa, respectively.[54, 55] Oxygen dissolved in metallic Cr can cut the hardness in half.[56]

The ternary WCN coatings were found to be highly adherent, but were the thinnest. The reactive gas (nitrogen) reduced the deposition rate, resulting in a film of only 0.9 μm. This thickness may also be a contributing factor in the lower hardness values. X-ray diffraction pattern of this material in Figure 1(c) shows a small diffraction peak at 44.6° from the Cr buffer layer. The WCN phase is characterized by a single broad peak at 34.9°. This peak's FWHM is 6.1° and rather symmetric, and using the Debye-Scherrer equation, the crystallite size is estimated at 1.6 nm. However, the broadness of this peak may be a result of an overlap of phases with locally varied composition and the presence of partially amorphous phase. In addition, film stress tends to broaden peaks. This analysis is somewhat consistent with WCN formation using a much lower N_2 partial pressure during sputtering.[57]

From the fitting of the high resolution XPS spectra (not shown), the C1s have three possible states at 284.9 eV, 283.6 eV, and 282.3 eV. The state at 284.9 eV is consistent with sp^2-bonded C within the film. The other carbon states at 283.6 eV and 282.3 eV are both carbides. Both nitrogen states, 396.5 eV and 395.4 eV, are bound in nitrides. The W4d spectra yield two states, and the W4f only one state. In addition, this film contains approximately 1 at.% of O1s. Furthermore, Raman spectroscopy results (not shown) indicated the presence of sp^2-bonded carbon. From these results, we determine the film consists of primarily WCN, with WO_x and sp^2-bonded C.

The nearly amorphous structure of the WCN coating can be responsible for the very low surface roughness of $R_{rms} = 1.28$ nm. Yet, the hardness and Young's modulus are only 11 GPa and 187 GPa, respectively. While there are several possible culprits for these low mechanical properties, there are three that stand out. The first is oxygen contamination. Hao et al.[58] have previously noted the detrimental effects of oxygen in Si-Ti-N based systems. The second is the effect of small film thickness on a relatively soft substrate.[49] In addition, the presence of free graphitic carbon phase can be another factor as this phase is expected to be relatively soft.

The composite coating prepared by the simultaneous sputtering of WC and Cr targets in an argon-nitrogen atmosphere was quite different from the materials discussed above. Both XPS and XRD suggest that CrWCN seems to be a true nanocomposite. The XRD patterns of CrWCN are very different from those for other samples.

Both the W4f (not shown) and N1s, Figure 3(a), are in one state. Figure 3(b) is the C1s, with two states located at 284.3 eV and 282.1 eV. Figure 3(c) shows the Cr2p peaks, deconvoluted into two distinct states. Figure 3(d) is the W4d which also shows two states. Due to thermodynamic considerations, it is expected for the nitrogen to bind primarily with Cr. Therefore, based on the XPS data, it has been suggested that this quaternary composite may be comprised primarily of two distinct WC and CrN nanocrystalline phases. Additionally, compositional analysis determined the Cr:W ratio is 1.94:1. This conclusion is partially supported by the XRD pattern in Figure 1(d), where the peaks from CrN and WC_{1-x} phases are close and overlap. The mean grain size of both phases seems to be similar, and in a 7–8 nm range.

The formation of a nanocrystalline composite material, with at least two phases, can be responsible for the improved mechanical and other characteristics of the CrWCN coatings when compared with other samples. These coatings are well adherent and very smooth with $R_{rms} = 1.65$ nm, as shown in Figure 4. The hardness and Young's modulus of CrWCN were determined as 27 GPa and 280 GPa, respectively.

While there are some interesting possibilities within coatings based on Cr-WC-N, this is only part of the overall picture. One targeted application for these coatings is the underlayers for successful nanocrystalline diamond (NCD) deposition. Each of the samples above, on Si substrates, were used to deposit NCD by microwave plasma assisted CVD. In these preliminary experiments, it has been found that both the WCN and CrWCN showed NCD layer growth without additional seeding. The binary WC and ternary CrWC samples delaminated during the NCD deposition. Figure 5 is the XRD patterns for both the (a) WCN and (b) CrWCN films after NCD deposition. In both films, there is a small peak at 44.4° which corresponds to (111) peak in diamond. The size of the diamond crystallites was estimated about 9 nm in both films. However, as can be seen in Figure 5(a), there is a phase transition from a nearly amorphous WCN film to a polycrystalline composite. Due to annealing, and the reducing effects of hydrogen during the NCD deposition, the ternary layer decomposes into WC_{1-x} (with a peak at 41.8°), W_2C (with peaks at 36° and 39.4°), and pure W (with a peak at 40.4°) phases. The CrWCN film (Fig. 5(b)) exhibits significantly different behavior. Based on the XRD data, it has been proposed that this nanocomposite decomposes into W_2C (peak at 36°), WC_{1-x} (peak at 41.3°), CrN (peaks at 37.8° and 43.4°), and possibly CrC (peak at 44.9°) nanocrystalline phases without significant changes in the surface morphology and adhesion.

The formation of NCD has been further confirmed with Raman spectroscopy, as shown in Figures 6(a, b). For ternary and quaternary based films, deposited on both Si and Ti, the NCD layers demonstrated the same Raman spectra with distinct peaks at 1135 cm^{-1}, 1331 cm^{-1},

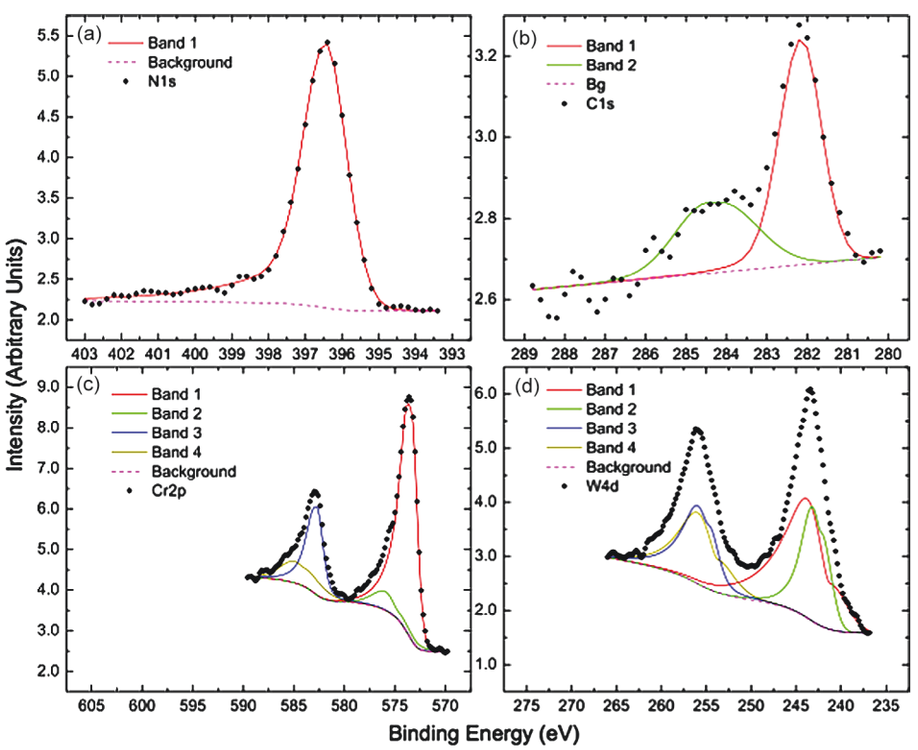

Fig. 3. X-ray photoelectron spectroscopy results for the (a) N1s, (b) C1s, (c) Cr2p, and (d) W4d peaks of the CrWCN coating, deposited on Si. The symbols (♦) are the raw data, with the deconvoluted peaks (solid) and the iterated Shirley background (dashed).

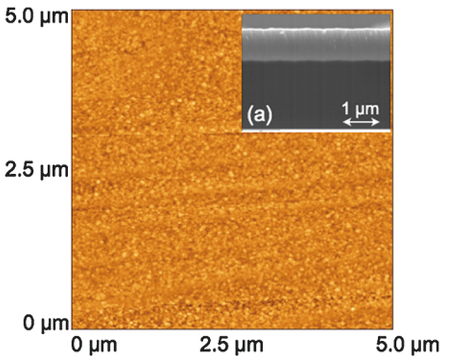

Fig. 4. Atomic force microscopy (5×5 μm^2) image of the CrWCN coating on Si, with the cross-section from high resolution scanning electron microscopy as the (a) inset.

1358 cm^{-1}, 1471 cm^{-1}, and 1536 cm^{-1}. The peak at 1331 cm^{-1} is due to diamond. The peaks at 1135 cm^{-1} and 1471 cm^{-1} are typically ascribed to polyacetylene chain fragments.[59, 60] The peaks at 1358 cm^{-1} and 1536 cm^{-1} are the D- and G-lines for small, distorted sp^2-bonded cluster.[61] The lack of significant line-shifts may correspond to low internal stress within the NCD layer.

However, the NCD does not form a smooth layer as seen in Figure 6(c). Prior to deposition, the surface roughness of the WCN and CrWCN coatings were 1.28 nm and 1.65 nm, respectively. After NCD deposition, both the WCN and CrWCN based films had surface roughness in excess of 30 nm. This can be a result of enhanced secondary nucleation during NCD growth. Since this occurs on both ternary and quaternary underlayers, the problem may lie within the NCD deposition process rather than the coating parameters.

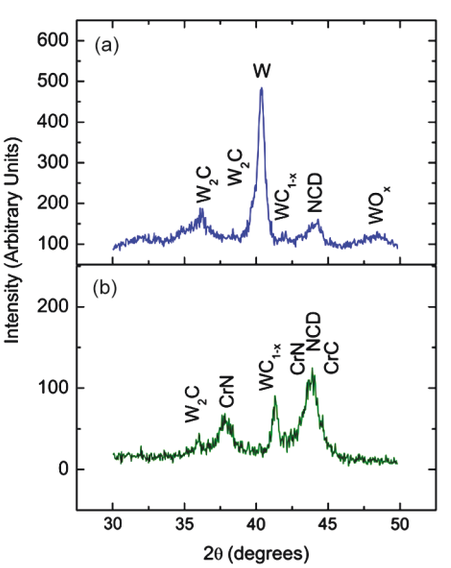

Fig. 5. X-ray diffraction patterns for the NCD films deposited on (a) the WCN coating and (b) the CrWCN coating, deposited on Si.

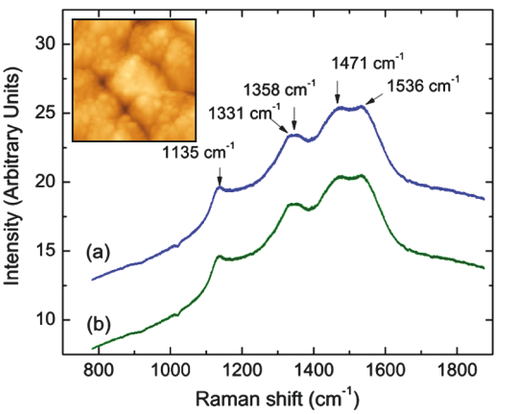

Fig. 6. Raman spectra (the excitation wavelength is 532 nm) for the NCD coatings on (a) the WCN coating and (b) the CrWCN coating, deposited on Si. The (c) inset is the AFM (5×5 μm^2) image of NCD layer on CrWCN layer.

4. CONCLUSION

Cr-WC-N based coatings were successfully deposited onto both Si and Ti substrates, using reactive RF magnetron sputtering. The binary WC films have the highest hardness, but these coatings partially delaminate from both Si and Ti substrates. The ternary Cr-WC films also show high hardness, with good adhesion. However, neither the WC nor the Cr-WC films survived the microwave plasma, and cannot support nanodiamond growth. The hardness of the ternary WCN films was lower, but the coating was adherent after plasma treatment, and supported nanodiamond growth. The CrWCN nanocomposite was also adherent after plasma treatment, with a much higher hardness than the WCN and Cr-WC coatings. Nanocrystalline diamond films were successfully deposited onto the quaternary CrWCN films. However, problems with secondary nucleation significantly increased the surface roughness of the nanocrystalline diamond films on both WCN and CrWCN. The NCD deposition process optimization will be required to verify the feasibility of using CrWCN and WCN films as underlayers for smooth NCD growth.

Acknowledgments: The authors would like to thank Jeff Montgomery at the University of Alabama at Birmingham for his assistance with Raman spectroscopy. This project was supported by US National Science Foundation grants (DMR-08606521 and DMR-0922910) and the Regional Council of Burgundy, France.

References and Notes

1. E. Posti and I. Nieminen, *Wear* 129, 273 **(1989)**.
2. H. I. Malik, R. Mgaloblishvili, and B. Mills, *J. Mater. Sci. Lett.* 19, 1779 **(2000)**.
3. M. Minn and S. K. Sinha, *Surf. Coat. Technol.* 202, 3698 **(2008)**.
4. Y. L. Su and W. H. Kao, *Wear* 223, 119 **(1998)**.

5. A. Stanishevsky and R. Lappalainen, *Surf. Coat. Technol.* 123, 101 **(2000)**.
6. S. A. Catledge, Y. K. Vohra, S. A. Catledge, and Y. K. Vohra, *J. Appl. Phys.* 84, 6469 **(1998)**.
7. S. A. Catledge, Y. K. Vohra, S. A. Catledge, and Y. K. Vohra, *J. Appl. Phys.* 86, 698 **(1999)**.
8. R. Haubner, S. Kubelka, B. Lux, M. Griesser, and M. Grasserbauer, *J. Phys. IV* 5, 753 **(1995)**.
9. N. M. Everitt, R. F. Silva, J. Vieira, C. A. Rego, C. R. Henderson, and P. W. May, *Diamond Relat. Mater.* 4, 730 **(1995)**.
10. S. Amirhaghi, H. S. Reehal, R. J. K. Wood, and D. W. Wheeler, *Surf. Coat. Technol.* 135, 126 **(2001)**.
11. H. Sein, W. Ahmed, M. Jackson, R. Polini, I. Hassan, M. Amar, and C. Rego, *Diamond Relat. Mater.* 13, 610 **(2004)**.
12. C. S. Abreu, M. Amaral, F. J. Oliveira, A. J. S. Fernandes, J. R. Gomes, and R. F. Silva, *Diamond Relat. Mater.* 15, 2024 **(2006)**.
13. S. Silva, V. P. Mammana, M. C. Salvadori, O. R. Monteiro, and I. G. Brown, *Diamond Relat. Mater.* 8, 1913 **(1999)**.
14. V. A. Silva, F. M. Costa, A. J. S. Fernandes, M. H. Nazaré, and R. F. Silva, *Diamond Relat. Mater.* 9, 483 **(2000)**.
15. N. Toprani, S. A. Catledge, Y. K. Vohra, and R. Thompson, *J. Mater. Res.* 15, 1052 **(2000)**.
16. W. L. Wang, K. J. Liao, and R. Q. Zhang, *Mater. Lett.* 44, 336 **(2000)**.
17. F. H. Sun, Z. M. Zhang, M. Chen, and H. S. Shen, *Diamond Relat. Mater.* 12, 711 **(2003)**.
18. F. Álvarez, M. Reinoso, H. Huck, and M. Rosenbusch, *Appl. Surf. Sci.* 256, 3962 **(2010)**.
19. Y. Tang, Y. S. Li, Q. Yang, and A. Hirose, *Thin Solid Films* 519, 1606 **(2010)**.
20. Q. P. Wei, Z. M. Yu, L. Ma, D. F. Yin, and J. Ye, *Appl. Surf. Sci.* 256, 1322 **(2009)**.
21. Y. S. Li, Y. Tang, Q. Yang, S. Shimada, R. Wei, K. Y. Lee, and A. Hirose, *Int. J. Refract. Met. Hard Mater.* 26, 465 **(2008)**.
22. Y. Li, Y. Gao, B. Xiao, T. Min, Z. Fan, S. Ma, and L. Xu, *J. Alloys Compd.* 502, 28 **(2010)**.
23. H. C. Chen, K. F. Liu, N. H. Tai, W. F. Pong, and I. Lin, *Diamond Relat. Mater.* 19, 134 **(2010)**.
24. J. Musil, *Surf. Coat. Technol.* 125, 322 **(2000)**.
25. A. Kumar, Q. You, J. S. Kapat, A. Mangiaracina, A. Catledge, and Y. Vohra, *Thin Solid Films* 308, 209 **(1997)**.
26. Y. Lifshitz, C. H. Lee, Y. Wu, W. J. Zhang, I. Bello, and S. T. Lee, *Appl. Phys. Lett.* 88, 243114 **(2006)**.
27. S. Veprek, A. Niederhofer, K. Moto, T. Bolom, H. D. Männling, P. Nesladek, G. Dollinger, and A. Bergmaier, *Surf. Coat. Technol.* 133, 152 **(2000)**.
28. S. Veprek and S. Reiprich, *Thin Solid Films* 268, 64 **(1995)**.
29. V. V. Brazhkin, A. G. Lyapin, and R. J. Hemley, *Philos. Mag. A* 82, 231 **(2002)**.
30. S. Veprek, M. G. J. Veprek-Heijman, P. Karvankova, and J. Prochazka, *Thin Solid Films* 476, 1 **(2005)**.
31. S. Veprek, H. D. Männling, A. Niederhofer, D. Ma, and S. Mukherjee, *J. Vac. Sci. Technol. B: Microelectron. Nanometer Struct.* 22, L5 **(2004)**.
32. S. Veprek, A. S. Argon, and R. F. Zhang, *Philos. Mag.* 90, 4101 **(2010)**.
33. A. A. Voevodin, S. V. Prasad, and J. S. Zabinski, *J. Appl. Phys.* 82, 855 **(1997)**.
34. A. A. Voevodin, J. P. O'Neill, and J. S. Zabinski, *Thin Solid Films* 342, 194 **(1999)**.
35. K. Fuchs, P. Rödhammer, E. Bertel, F. P. Netzer, and E. Gornik, *Thin Solid Films* 151, 383 **(1987)**.
36. J. Esteve, G. Zambrano, C. Rincon, E. Martinez, H. Galindo, and P. Prieto, *Thin Solid Films* 373, 282 **(2000)**.
37. Y. Gachon, P. Ienny, A. Forner, G. Farges, M. C. S. Catherine, and A. B. Vannes, *Surf. Coat. Technol.* 113, 140 **(1999)**.
38. T. Polcar, N. M. G. Parreira, and A. Cavaleiro, *Wear* 262, 655 **(2007)**.
39. T. Polcar, N. M. G. Parreira, and A. Cavaleiro, *Wear* 265, 319 **(2008)**.
40. T. Polcar and A. Cavaleiro, *Int. J. Refract. Met. Hard Mater.* 28, 15 **(2010)**.
41. L. Swadzba, A. Maciejny, B. Formanek, P. Liberski, P. Podolski, B. Mendala, H. Gabriel, and A. Poznanska, *Surf. Coat. Technol.* 78, 137 **(1996)**.
42. I. Milosev, H. Strehblow, and B. Navinsek, *Thin Solid Films* 303, 246 **(1997)**.
43. P. Hones, N. Martin, M. Regula, and F. Levy, *J. Phys. D: Appl. Phys.* 36, 1023 **(2003)**.
44. R. Daniel, K. J. Martinschitz, J. Keckes, and C. Mitterer, *J. Phys. D: Appl. Phys.* 42, 075401 **(2009)**.
45. Q. Liang, S. A. Catledge, and Y. K. Vohra, *Appl. Phys. Lett.* 83, 5047 **(2003)**.
46. Q. Liang, A. Stanishevsky, and Y. K. Vohra, *Thin Solid Films* 517, 800 **(2009)**.
47. S. Chowdhury, J. Borham, S. A. Catledge, A. W. Eberhardt, P. S. Johnson, and Y. K. Vohra, *Diamond Relat. Mater.* 17, 419 **(2008)**.
48. W. C. Oliver and G. M. Pharr, *J. Mater. Res.* 7, 1564 **(1992)**.
49. X. Chen and J. J. Vlassak, *J. Mater. Res.* 16, 2974 **(2001)**.
50. ICDD, Powder Diffraction File Inorganic and Organic Data Book, edited by S. Kabekkodu (International Center for Diffraction Data, Newtown Square, PA **2007**).
51. Z. A. Hamid, I. M. Ghayad, and K. M. Ibrahim, *Surf. Interface Anal.* 37, 573 **(2005)**.
52. M. Brieseck, M. Bohn, and W. Lengauer, *J. Alloys Compd.* 489, 408 **(2010)**.
53. NIST X-ray Photoelectron Spectroscopy Database, Version 3.5 (National Institute of Standards and Technology, Gaithersburg, **2003**); http://srdata.nist.gov/xps/.
54. N. M. G. Parreira, N. J. M. Carvalho, and A. Cavaleiro, *Thin Solid Films* 510, 191 **(2006)**.
55. N. M. G. Parreira, N. J. M. Carvalho, F. Vaz, and A. Cavaleiro, *Surf. Coat. Technol.* 200, 6511 **(2006)**.
56. P. Hones, M. Diserens, and F. Lévy, *Surf. Coat. Technol.* 120, 277 **(1999)**.
57. S. I. Kim and C. W. Lee, *Phys. Status Solidi C* 4, 4475 **(2007)**.
58. S. Hao, B. Delley, S. Veprek, and C. Stampfl, *Phys. Rev. Lett.* 97, 86102 **(2006)**.
59. C. Castiglioni, M. Tommasini, and G. Zerbi, *Philos. Trans. A: Math. Phys. Eng. Sci.* 362, 2425 **(2004)**.
60. A. C. Ferrari and J. Robertson, *Phys. Rev. B* 63, 121405 **(2001)**.
61. A. C. Ferrari and J. Robertson, *Philos. Trans. A: Math. Phys. Eng. Sci.* 362, 2477 **(2004)**.